

## Enhanced soil profile visualization using portable X-ray fluorescence (PXRF) spectrometry



Fujun Sun<sup>a</sup>, Noura Bakr<sup>b</sup>, Tommy Dang<sup>c</sup>, Vung Pham<sup>c</sup>, David C. Weindorf<sup>d,\*</sup>, Zhuodong Jiang<sup>a</sup>, Hualei Li<sup>a</sup>, Qiu-Bing Wang<sup>a</sup>

<sup>a</sup> College of Land and Environment, Shenyang Agricultural University, Shenyang, China

<sup>b</sup> Soils and Water Use Department, National Research Centre, Cairo, Egypt

<sup>c</sup> Department of Computer Science, Texas Tech University, Lubbock, TX, USA

<sup>d</sup> Department of Plant and Soil Science, Texas Tech University, Lubbock, TX, USA

### ARTICLE INFO

Handling Editor: Alex McBratney

Keywords:

Pedology

Soil profile description

Elemental data

Proximal sensors

Pedometrics

### ABSTRACT

Soil horizonation has traditionally relied upon morphological description, field sampling, and laboratory analysis as a means of establishing key diagnostic horizons and features within a soil profile. While this technique is useful for many soil properties, other quantifiable properties associated with elemental abundance may be visually imperceptible. Portable X-ray fluorescence (PXRF) spectrometry allows for rapid elemental data acquisition *in-situ*, providing more than 20 elements commonly detectable within a soil profile. In this study, a grid containing 130 cells was physically imposed upon two soil profiles in West Texas, USA. PXRF was used to sequentially scan each grid cell and acquire elemental data. The profiles were morphologically described by a panel of soil scientists, sampled, and subjected to traditional laboratory characterization. Data from the PXRF and field sampling were statistically compared, then visualized as depth functions. A data visualization tool was created to overlay elemental data on top of a digital photograph of the soil profile in semitransparency. Using elemental data as a proxy, PXRF data was able to detect both argillic and calcic horizons within one soil profile and visually illustrate their extent and assist in delineating horizons in a second profile with nondescript horizons. The soil visualization tool has other features as well such as correlation analysis between elements, adjustable correlation threshold in real time, rasterized vs. smoothed data overlay, and box-plots of elemental concentrations. Summarily, this research developed a new tool for PXRF data visualization in support of soil pedon description, allowing for elemental data which may be visually imperceptible to be considered during soil profile characterization. Future advancements will seek to integrate this tool directly into the PXRF software for on-site visualization of any element specified by the analyst. Applications of such could include real-time mapping of contaminant metals in soil profiles.

### 1. Introduction

Since the inception of soil morphology and classification, various soil properties have been used as differentia for uniquely identifying soils. Physical characteristics such as sand/silt/clay content, color, and structural aggregation are commonly used characteristics by which soil horizons are recognized and described. Additionally, certain chemical features such as soil reaction (pH) and salinity are used in a similar manner. For example, salic horizons, sulfidic materials, and sulfuric horizons are all examples of chemical properties used by the [Soil Survey Staff \(2014a\)](#) to characterize soil profiles. However, recent studies have also established the utility of proximal sensors (e.g., portable X-ray

fluorescence spectrometry - PXRF; visible near infrared diffuse reflectance spectroscopy – VisNIR DRS) in delineating soil horizons, properties, and features within a given profile. For example, [Weindorf et al. \(2012\)](#) used PXRF to enhance the morphological expression of nondescript Inceptisols in Louisiana, USA. Following on, [Weindorf et al. \(2015\)](#) used both PXRF and VisNIR DRS for identification of lithologic discontinuities in the USA, Hungary, and Italy. [Silva et al. \(2018\)](#) used PXRF for characterization of tropical soil weathering in the Brazilian Cerrado. Finally, [Chakraborty et al. \(2017\)](#) utilized PXRF to establish the developmental stage of secondary carbonates (calcic/petrocalcic horizons) in soils of Texas, Kansas, Colorado, and New Mexico. PXRF is rapidly gaining popularity for soil analysis owing to its ease of use and

\* Corresponding author.

E-mail address: [david.weindorf@ttu.edu](mailto:david.weindorf@ttu.edu) (D.C. Weindorf).

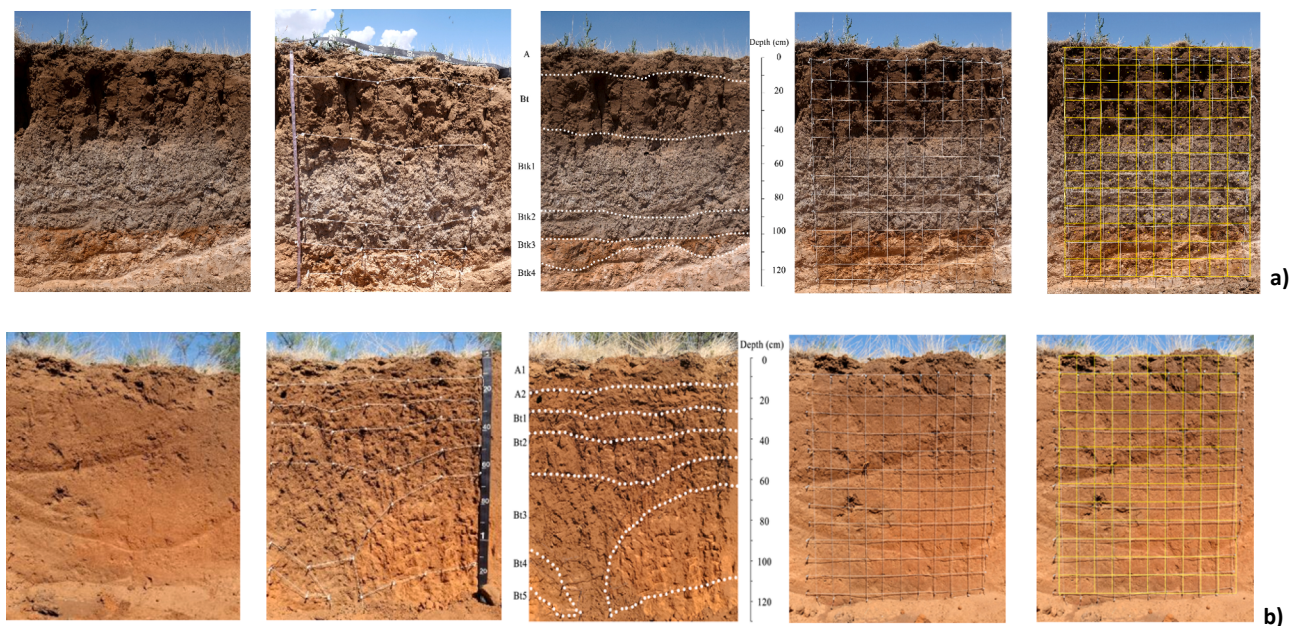


**Fig. 1.** Soil profile ( $130 \times 100$  cm) horizons for field description and grid cells for scanning ( $10 \times 10$  cm) in Lubbock, TX, USA. a) Profile 1; b) profile 3.

non-destructiveness. The [Soil Survey Staff \(2014b\)](#) recognizes it as an approved method in the *Soil Survey Field and Laboratory Methods Manual*, and recent soil investigations have applied the instrument for soil geochemical and pollutant characterization ([Lemière, 2018](#); [Hu et al., 2017](#); [Jang, 2010](#)).

While soil horizons and associated taxa have traditionally been established upon morphological characteristics and supporting laboratory data, there is no rule against establishing differentia based upon fundamental (elemental) chemistry in soils. [Weindorf et al. \(2012\)](#) alluded to this directly stating “The authors do not endorse the strict use of PXRF elemental data for soil horizon establishment, irrespective of morphological features. Rather, PXRF is suggested as a tool for enhancing field morphological horizonation.” However, proximal sensors such as PXRF do offer insight into differences within a soil profile that may be visually imperceptible. For example, [Zhu et al. \(2011\)](#) studied differences in soil texture using Fe and Rb as indicators of soil clay content. [Sharma et al. \(2015\)](#) established the efficacy of using PXRF for soil cation exchange capacity prediction relating elemental concentrations and laboratory data via multiple linear regression. Finally, [Rawal et al. \(2019\)](#) used four multivariate approaches to predict soil base saturation percentage in temperate agricultural soils of the USA. In fact, future taxa currently under development for *US Soil Taxonomy* describing human altered/human transported (HAHT) soils may require the development of new methodological approaches for characterization; PXRF has the potential to meet certain aspects of that forthcoming need (John Galbraith, personal communication).

Early versions of PXRF equipment established a basic field portable unit capable of scanning soil on site. Technological advances led to several generations of the equipment ([Weindorf et al., 2014](#)) with newer features such as Bluetooth connectivity, integrated global positioning system (GPS) receiver, and on-board digital cameras now common among many manufacturers. These advances have provided new possibilities for applying PXRF technology to soil profile characterization and innovative ways of visualizing the elemental data provided by such, for the benefit of field soil scientists. The objectives of this study were to: 1) compare traditional soil morphological description to PXRF elemental profile data using newly developed data visualization tools, and 2) establish a variety of new data interfaces such that PXRF data may be more meaningfully interpreted on-site. We hypothesize that the PXRF data visualization tool will provide valuable

insight into soil properties identifying both visually perceptible and imperceptible features within soil profiles.

## 2. Materials and methods

### 2.1. General occurrence and features of soils in this study

Three soil profiles were evaluated for this study, yet given the voluminous amount of data generated, profile 1 was used as an example for discussion with additional data from profile 3 used for comparison. While showing substantive variation in morphological expression, both profiles presented are consistent with the Amarillo series (Fine-loamy, mixed, superactive, thermic Aridic Paleustalf), a recognized benchmark soil series of Texas. Both soil profiles were located on the Texas Tech University Erskine Experimental Rangeland in Lubbock, TX, USA ( $33^{\circ} 36' 10''$  N;  $101^{\circ} 54' 00''$  W) and were excavated with a backhoe to form a small pit. Elevation was  $\sim 2600$  m ASL. Located in Major Land Resource Area 77C ([Soil Survey Staff, 2006](#)), the rangeland features small grass prairie (blue grama, *Bouteloua gracilis*; buffalograss, *Bouteloua dactyloides*), invasive honey mesquite (*Prosopis glandulosa*), and a depressional playa. The area features an ustic moisture regime (405–560 mm annual precipitation) and thermic temperature regime with prevailing winds out of the south ([Soil Survey Staff, 2006](#)).

### 2.2. Field characterization

The soil pits were excavated to a depth of 1.3 m in Summer, 2018. The pit faces were cleaned with a small knife in preparation for description after being allowed to dry for several days under ambient conditions. Prior to morphological description, string was used to physically impose a grid across each profile; each grid cell was  $10 \text{ cm}^2$ . So both soil profile walls were divided into  $1.0 \times 1.3 \text{ m}$  rasters of  $10 \times 10 \text{ cm}$  squares to a depth of 1.3 m (Fig. 1).

A column and row numbering system was established, such that each grid cell had a unique identifier. Digital photographs were taken of each soil profile. Then, a Vanta Series M PXRF (Olympus, Waltham, MA, USA) was used to scan the center of each  $10 \times 10 \text{ cm}$  cell *in-situ* ([Soil Survey Staff, 2014b; US EPA, 2007](#)); the scanning area of the instrument is  $\sim 1.5 \text{ cm}^2$ . The instrument was calibrated with a 316 standard alloy and operated in *Geochem Mode* at  $45 \text{ s beam}^{-1}$  such that one

complete scan was completed in 90 s. Sequentially, each cell of the grid across both profiles was scanned. Instrument performance was verified by scanning National Institute of Standards and Technology (NIST) certified reference materials, with recovery percentage calculated as PXRF reported versus certified reference value on an element by element basis (Koch et al., 2017).

Following PXRF scanning, a panel of five soil scientists morphologically evaluated the profile per Schoeneberger et al. (2012). Color measurements were taken using Munsell soil color charts. Pedogenic features such as secondary carbonates, clay films, redox features, and sesquioxide nodules were assessed. A small knife and hand trowel were used to collect samples from each morphologically established horizon of the pit. Samples were placed in sealed plastic bags for transport to the laboratory.

### 2.3. Laboratory characterization

Prior to analysis, all samples were air dried and disaggregated to pass a 2 mm sieve. Particle size analysis was conducted per Gee and Bauder (1986) using a model 152-H hydrometer and 1440 min for clay determination; 40 s readings were used for sand determination. For soil reaction (pH) and electrical conductivity (EC) determination, a 1:1 soil:water (v/v) slurry was made, allowed to equilibrate for 30 min, then determined electrometrically (Thomas, 1996). Soil organic matter was determined via loss on-ignition at 400 °C for 16 h in a muffle furnace (Nelson and Sommers, 1996).

### 2.4. Data analysis

At the beginning of the data analysis, outliers were identifying and then excluded from each dataset for the profile as they affect variogram behavior (McGrath and Zhang, 2003). A box-plot was performed for each studied element to examine the outliers as recommended by several studies (e.g., Zhang et al., 2009; Fu et al., 2016; Bakr and Al-Ashry, 2018). Box-plots are generally considered a standardized methodology for graphically displaying the statistical distribution of the dataset. Box plots note the first and third quartiles, representing 25 and 75% of the dataset at lower and upper boundaries, respectively. A line inside the box is the median of the dataset. This box is further bounded by two error bars (known as whiskers) above and below it; their limits indicate the maximum and minimum values, respectively. Samples above the whisker limits are considered outliers. For this research, only the 5th and 95th percentile were observed below and above error bars, respectively.

After the data was cleaned by removing outliers and elements which fell below the PXRF limit of detection (LOD) values, the continuous values of 20 elements (Si, Al, K, Mn, Fe, Ti, Cr, Cu, Nb, Zn, Rb, V, Y, Pb, Zr, S, Th, Ni, Ca, and Sr) were calculated using an equal area smoothing spline function (Bishop et al., 1999; Malone et al., 2009) and plotted using the ggplot2 R package (R Core Team, 2018). The equal-area smoothing spline function considers continuous soil property vertical trends within a soil profile whereby a pedologist can correlate soil properties and soil weathering indices to the degree of soil development, as well as soil-forming processes (Minasny et al., 2016).

In order to compare the grid data to the field-delineated horizons, a column of grid data by PXRF were assigned to soil horizons based on the boundaries. Since most of the grid scanning was taken from the center of each 10 × 10 cm cell and the scanning area of the PXRF is ~1.5 cm<sup>2</sup> (1.5% of each cell), the intervals containing horizon boundaries were considered to occur within a horizon only if the boundary occurred > 5 cm from the depth interval boundary. The average value of this column of data in an occurrence layer serves as the result of element content in the upper layer. Because some previous studies (e.g., Stockmann et al., 2016) have proved that the results of *in-situ* measurement are somewhat different from the results of air-dried samples in the laboratory, such treatment ensures that the data reflect the same test conditions.

### 2.5. Depth function curve between morphological horizons and fixed depth sampling

The elemental contents of samples collected from six morphologically established soil horizons and 10 cm depth-increment samples were analyzed. Then the depth function curves of each element on the soil profile were established according to the analysis results. To quantify the goodness-of-fit between the 10 cm depth-increment samples across 13 layers versus the traditional 6 morphological horizons of the profile, an R-square score (Nagelkerke, 1991) was calculated. The R-square score was used because it gives an estimate of the relationship between the movements of the two measurement types. An R-square score of 1.0 represents a perfect match, whereas a score of 0.0 represents a poor match (as simple as comparing one curve with a line representing the mean of another line). Also, it provides sufficient generality (Cameron et al., 1997) to reasonably address the correlation between these two non-linear curves.

### 2.6. Spatial analysis of soil profile elements

Digital photos for each studied profile were obtained using a FUJIFILM X-E2 camera. The digital photos were transferred to ArcMap then cropped and georeferenced to the profile face (100 × 130 cm). A semivariogram of each soil element for the profile was developed to determine spatial dependence and a continuous two-dimensional surface. Different semivariogram models were examined to measure the spatial correlation between the two points and select the best fitting model based on the variogram parameters (mainly; nugget, sill, and range). As each soil profile was scanned in the 10 × 10 cm grid cells (n = 130), ordinary kriging interpolation was used to investigate the spatial distribution of the 20 scanned elements. Ordinary kriging considers the best linear unbiased estimator as it minimizes the error variance, estimates weighted linear combination, and obtains the mean residual equal to zero (Kiš, 2016). The best fit kriging model was examined by calculating the root mean squared error (RMSE).

### 2.7. Visualization tool development

The visualization was developed using D3, Data-Driven Document, (Bostock et al., 2011) and Plotly (Sievert et al., 2016). Fig. 2 shows the operational theory of the data visualization tool. The tool calculates the sample correlations (Snedecor et al., 1980) among the elements to generate a force-directed network graph (Bostock et al., 2011) to show the relationships among them. This visual analytics solution aims to provide soil scientists with valuable insight into soil properties both visually perceptible with graphs and imperceptible features with statistical calculations. These are realized in several stages including data processing, data visualizations, and interactions (Ceneda et al., 2017).

At the data processing step, after the data is imported from the PXRF device, the data is then cleaned such as removing missing or < LOD values. Besides the 20 detected elements after cleaning, weathering indices and elemental trends such as the Ruxton Weathering Index, Desilication Index, and Stable Ratio are calculated and added to the soil profile to aid in soil properties analysis. The statistical modules help to compute several statistics to support the visual interface and the quantification of the analyzing feature.

To implement the analysis task, the visualization tool provides several interconnected views (Roberts, 2007) such as correlation graphs, scatter plots and linear regression line, contour-map/heat-map, box-plots, and goodness-of-fit line-graphs. The correlation graphs give an overview of all detected chemical elements and their relationships. The statistical modules calculate the sample correlations among the elements, the weathering indices, and elemental trends to generate a force-directed network graph. Also, a linear regression line further represents the estimated correlation. The statistical calculation of the correlation score is also displayed on top of the visualization to quantify

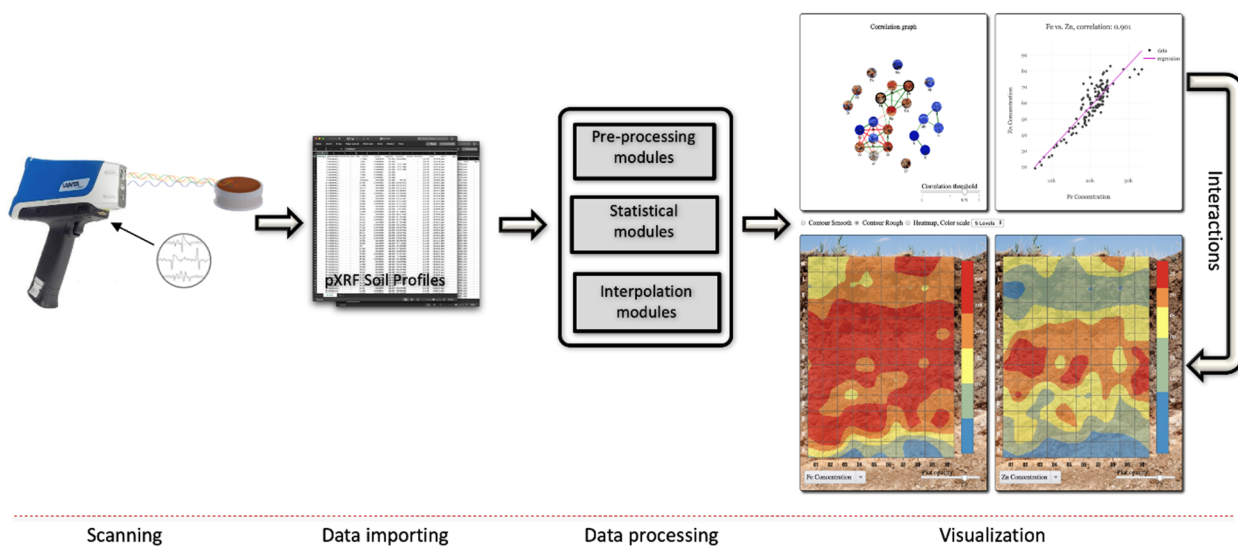


Fig. 2. Schematic overview of the data visualization tool.

the relationship. The contour-map/heat-map reproduces spatial distributions of the element concentrations over the 2D surface of the pit. In the case of the contour map, the data is first interpolated via kriging.

In contrast, the heat map shows the discrete data scanned from the corresponding cells. The box-plots show distributions of the selected elements across the soil horizons. Also, using box-plots allows for detection and removal of outlying data before applying other analysis techniques. The goodness-of-fit line-graphs compare the horizon analysis using morphologically established horizons versus the 10 cm depth-increment samples evaluation of multiple elements. The R-squared score is calculated and displayed on top of the element profile to quantify the goodness-of-fit.

This tool provides interactions to aid in the analysis process. The interactive features are best explained by experiencing the visualization tool at this address: <https://idatavisualizationlab.github.io/Soil/demos.html>. Users can select any uploaded PXRF soil horizon profile to visualize from the top menu. All the views are interconnected, for instance, users can choose any two nodes on the network graph, and the corresponding views will be updated to compare the two selected elements. Similarly, users can also choose individual chemical elements (or compounds) to analyze from the selection boxes at the bottom of the heat map view. There are also several interactions to customize individual views. On the correlation network graph, users can use a slider to set the correlation threshold. The network graph only shows the links for nodes with absolute values of the correlations greater than or equal to the user-specified threshold. At the bottom of the contour map/heat map view, there are sliders for the user to set the opacity of these graphs. Also, users can select three different color ranges from coarse (5 color ranges), fine (10 color ranges), and smooth (20 color ranges) from the top of the contour map/heat map view to differentially illustrate elemental levels.

### 3. Results and discussion

#### 3.1. Soil morphological description

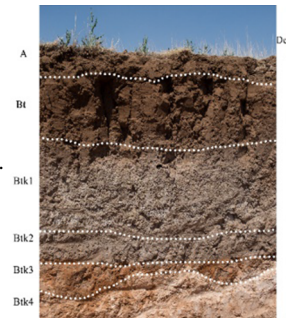
According to the characteristics of soil color, structure, texture, and other features, profile 1 was morphologically divided into six horizons, namely A, Bt, Btk1, Btk2, Btk3 and Btk4 (Fig. 1a) while profile 3 was morphologically divided into seven horizons, namely A1, A2, Bt1, Bt2, Bt3, Bt4 and Bt5 (Fig. 1b). Description were based on the *Field Book for Describing and Sampling Soils* version 3.0 (Schoeneberger et al., 2012). In this paper, profile 1 was used as an example for discussion, with additional data from profile 3 used for comparison as "Part b" of Tables 1, 2 and 3.

In profile 1, the second to last horizon had a hue of 5YR and value of 4, while the others had a hue of 7.5YR and value increased with depth. The chroma of the bottom two soil horizons was the highest, and the others increased slightly with depth (Table 1a). Data for profile 3 provided for comparison in Table 1b.

Clay content was highest in the Btk1 horizon (40–84 cm depth) and lowest in the Btk2 horizon (84–99 cm depth) (Table 2a). The former clearly met the requirements of an argillic horizon. Sand content followed the reverse pattern of clay content; silt content was fairly uniform vertically in the profile. The A horizon texture was loam, Btk1 was clay loam associated with the higher clay content, and all other horizons were sandy clay loam. Soil organic matter was highest in the A horizon and decreased with the depth. Except for the Btk2 horizon, soil pH increased with depth. In general, the pH of this profile was high owing to the calcic horizon deep in the profile. Data for profile 3 provided for comparison in Table 2b.

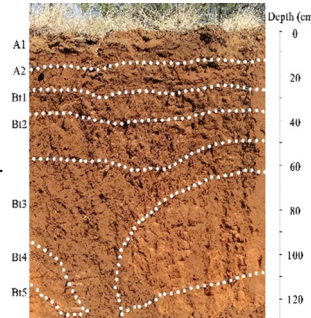
Because PXRF has different detection limits for each element based on unique electron configurations, it is not advisable to analyze for those elements whose detected values and limit of detection are close to each other. Statistically, there were 20 elements whose variation range exceeds the detection limit: Si, Al, Fe, Ca, K, Ti, Mn, Zr, S, Sr, Rb, V, Zn, Cr, Ni, Cu, Y, Pb, Nb, and Th. These 20 elements were roughly divided into three groups according to their elemental abundance. The highest elemental concentrations were for Si, Al, Fe, Ca, K, and Ti, expressed in percentage (%). All remaining elements were generally < 400 mg/kg (Tables 3a and 3b).

Since the profile was divided into six morphological soil horizons, the depth function of each element on the profile was calculated from six data which are the averages of the respective horizon. These elements can be divided into five groups according to the curve character of element content changing with depth. The first group includes Si, Al, Fe, K, Ti, Mn, and Cr, which were characterized by generally stable content from the surface downward in the profile; a small decrease in elemental abundance was evident deep in the profile (Fig. 3a). The second group consisted of Cu, Nb, Zn, Rb, V, and Y; their contents generally reached maximum concentration in the middle of the soil profile (e.g., argillic horizon) (Fig. 3b). The third group of elements (S, Zr, Pb) showed a general steady decline from the surface with depth (Fig. 3c). The fourth group (Ni, Th) increased slightly from the surface with depth (Fig. 3d). The last group (Ca, Sr) increased dramatically deep in the profile (Fig. 3e).

**Table 1a**

Selected morphological features of soil profile 1 studied in Lubbock, TX, USA.

Horizon	Depth cm	Boundary <sup>1</sup>	Color Moist	Structure <sup>2</sup>	Consistence <sup>3</sup> Dry	Roots <sup>4</sup>	Texture <sup>5</sup>
A	0–15	C S	7.5YR 3/4	2, M, SBK	SH	C Fi	L
Bt	15–40	C S	7.5YR 3/4	2, M, PR → 2, M, SBK	MH	C Fi	SCL
Btk1	40–84	C S	7.5YR 5/3	1, M, PR → 3, M, SBK	HA	C Fi	CL
Btk2	84–99	A S	7.5YR 5/3	3, F, ABK	EH	F Fi	SCL
Btk3	99–117	A W	5 YR 4/6	3, M, ABK	EH	F Fi	SCL
Btk4	117–130	—	7.5YR 6/6	2, M, SBK	SH	F Fi	SCL

**Table 1b**

Selected morphological features of soil profile 3 studied in Lubbock, TX, USA.

Horizon	Depth cm	Boundary <sup>1</sup>	Color Moist	Structure <sup>2</sup>	Consistence <sup>3</sup> Dry	Roots <sup>4</sup>	Texture <sup>5</sup>
A1	0–12	C S	7.5YR 4/3	2, M, SBK	SH	C Fi	FSL
A2	12–24	C S	7.5YR 4/3	2, C, PR → 2, M, SBK	H	C Fi	SCL
Bt1	24–34	C S	5 YR 4/3	2, C, PR → 2, M, SBK	H	C Fi	SCL
Bt2	34–47	CS	5 YR 4/3	2, C, PR → 2, M, SBK	H	C Fi	SCL
Bt3	47–63	C W	5 YR 4/4	1, C, PR → 2, M, SBK	H	C Fi	SCL
Bt4	63–114	GW	5 YR 4/6	1, C, PR → 2, M, SBK	H	C Fi	SCL
Bt5	114–130	—	5 YR 4/6	1, C, PR → 2, M, SBK	H	C Fi	SCL

<sup>1</sup> C = clear; A = abrupt; S = smooth; W = wavy.

<sup>2</sup> 1 = weak; 2 = moderate; 3 = strong; M = moderate; F = fine; SBK = subangular blocky; ABK = angular blocky; PR = prismatic.

<sup>3</sup> SH = slightly hard; MH = moderately hard; HA = hard; EH = extremely hard.

<sup>4</sup> C = common; F = few; Fi = fine.

<sup>5</sup> L = loam; SCL = sandy clay loam; CL = clay loam.

**Table 2a**

Physicochemical properties of soil profile 1 studied in Lubbock, TX, USA.

Horizon	Depth cm	pH	EC <sup>1</sup> μS/m	SOC %	Sand %	Silt	Clay
A	0–15	7.75	351	1.85	49.81	30.03	20.16
Bt	15–40	7.86	331	1.24	49.73	24.06	26.21
Btk1	40–84	8.07	439	1.19	29.74	42.07	28.19
Btk2	84–99	7.94	477	0.73	56.03	15.94	28.03
Btk3	99–117	8.18	484	0.63	49.99	23.94	26.07
Btk4	117–130	8.53	371	0.46	51.91	21.97	26.11

**Table 2b**

Physicochemical properties of soil profile 3 studied in Lubbock, TX, USA.

Horizon	Depth cm	pH	EC <sup>1</sup> μS/m	SOC %	Sand %	Silt	Clay
A1	0–12	7.25	297	1.36	69.88	15.99	14.13
A2	12–24	7.11	233	0.87	70.02	15.91	14.06
Bt1	24–34	6.98	183	0.96	69.8	12.02	18.18
Bt2	34–47	6.89	184	1.19	61.82	16.01	22.16
Bt3	47–63	7.09	195	1.36	59.81	14.02	26.18
Bt4	63–114	7.43	174	0.88	65.87	9.997	24.14
Bt5	114–130	7.86	250	0.48	71.83	12.01	16.16

<sup>1</sup> EC = electrical conductivity; SOC = soil organic carbon.

**Table 3a**

Mean elemental content in horizons of soil profile 1 studied in Lubbock, TX, USA.

Horizon	Depth	Si	Al	Fe	Ca	K	Ti	Mn	Zr	S	Sr	Rb	V	Zn	Cr	Y	Ni	Cu	Pb	Nb	Th
		%	mg/kg																		
A	0–15	26.05	6.49	1.93	0.26	1.48	0.36	370.00	339.10	283.90	79.73	72.07	62.80	55.87	40.70	21.77	18.39	18.70	18.57	13.50	10.93
Bt	15–40	26.65	6.67	2.13	0.49	1.46	0.36	368.36	288.14	202.46	85.16	79.32	66.68	57.12	43.34	22.90	21.00	21.38	16.18	15.54	12.22
Btk1	40–84	24.81	5.85	2.36	1.74	1.43	0.38	341.49	257.63	191.64	123.06	89.06	72.53	70.06	47.19	25.70	20.95	24.03	18.49	18.27	15.25
Btk2	84–99	25.25	6.07	2.13	1.41	1.42	0.35	332.75	275.30	120.25	112.76	74.80	67.67	62.54	48.56	23.85	22.26	21.66	14.66	15.24	12.84
Btk3	99–117	20.67	5.58	1.94	5.88	1.16	0.27	284.98	232.86	145.93	140.47	61.58	58.01	52.61	41.24	17.10	26.32	18.38	11.38	11.41	12.23
Btk4	117–130	13.62	3.43	1.26	13.81	0.76	0.19	173.78	179.80	195.50	204.64	42.15	50.34	35.55	38.43	12.37	20.49	13.30	8.65	8.70	12.69

**Table 3b**

Mean elemental content in horizons of soil profile 3 studied in Lubbock, TX, USA.

Horizon	Depth	Si	Al	Fe	Ca	K	Ti	Zr	Mn	S	Sr	Rb	V	Zn	Cr	Y	Ni	Cu	Nb	Pb	Th	
		%	mg/kg																			
A1	0–12	27.15	5.85	1.41	—	—	1.22	0.32	311.95	280.22	203.23	57.15	51.18	49.67	33.77	31.38	16.17	15.20	14.97	12.22	11.85	11.65
A2	12–24	27.82	6.23	1.57	—	—	1.26	0.32	302.70	270.13	160.80	56.33	54.83	52.60	36.33	37.30	16.63	15.60	15.30	12.02	11.00	11.03
Bt1	24–34	27.03	6.82	1.84	—	—	1.27	0.32	289.98	279.08	146.28	59.92	63.02	53.64	43.36	43.88	17.18	17.64	15.62	12.20	11.92	9.11
Bt2	34–47	26.13	7.20	2.07	—	—	1.30	0.32	287.80	277.73	157.26	64.92	70.33	57.21	49.78	42.79	17.71	19.45	16.80	12.89	12.85	9.23
Bt3	47–63	25.70	7.47	2.25	—	—	1.35	0.33	299.27	291.38	162.39	69.36	75.34	59.58	54.51	46.38	18.90	21.06	19.69	13.90	13.91	11.40
Bt4	63–114	26.32	7.15	2.01	—	—	1.34	0.31	282.36	258.73	113.14	65.56	67.68	57.85	47.65	39.48	17.68	19.61	17.16	12.79	12.51	10.48
Bt5	114–130	27.16	6.53	1.64	—	—	1.27	0.29	279.59	202.15	98.63	59.13	56.93	46.49	38.09	34.17	15.65	17.41	14.44	11.61	10.91	10.42

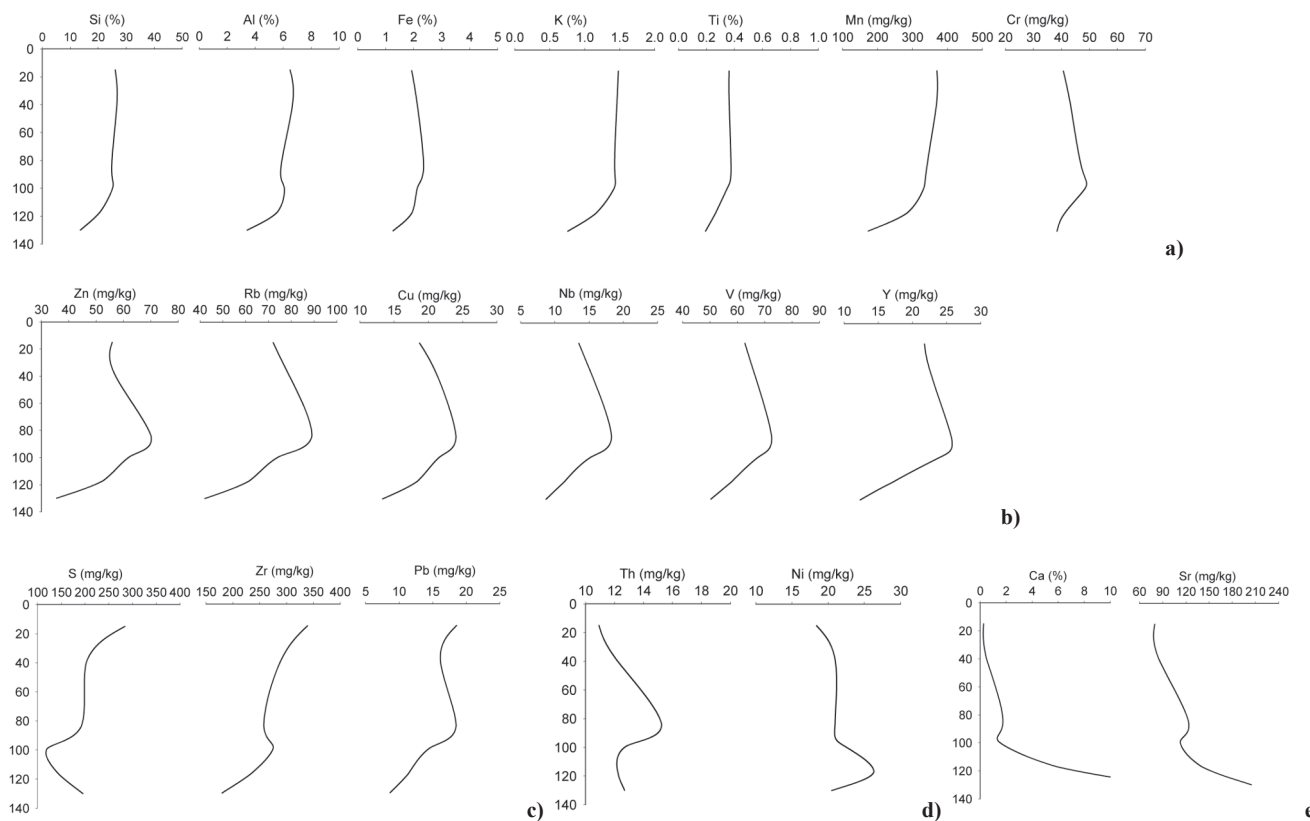


**Fig. 3.** Continuous depth function of soil elemental content for soil profile 1 in Lubbock, TX, USA. a) Group Si, Al, Fe, K, Ti, Mn, and Cr are generally stable from the surface downward in the profile with a small decrease in elemental abundance was evident deep in the profile; b) Cu, Nb, Zn, Rb, V, and Y generally reached maximum concentration in the middle of the soil profile (e.g., argillic horizon); c) S, Zr, Pb showed a generally steady decline from the surface with depth; d) Ni and Th increased slightly from the surface with depth; e) Ca and Sr increased dramatically deep in the profile.

### 3.2. Fixed depth profile variability

Hartemink and Minasny (2014) indicated the potential for *in-situ* digital morphometrics for all attributes of a soil profile to give continuous depth functions of soil properties, when small depth increments

were sampled and analyzed. According to the statistics of the ten test results for every 10 cm depth of the section, there are 13 groups generating 130 data points in the profile which can be used to calculate the depth function of each element. Compared to using the results of morphological horizons to represent the average level of element

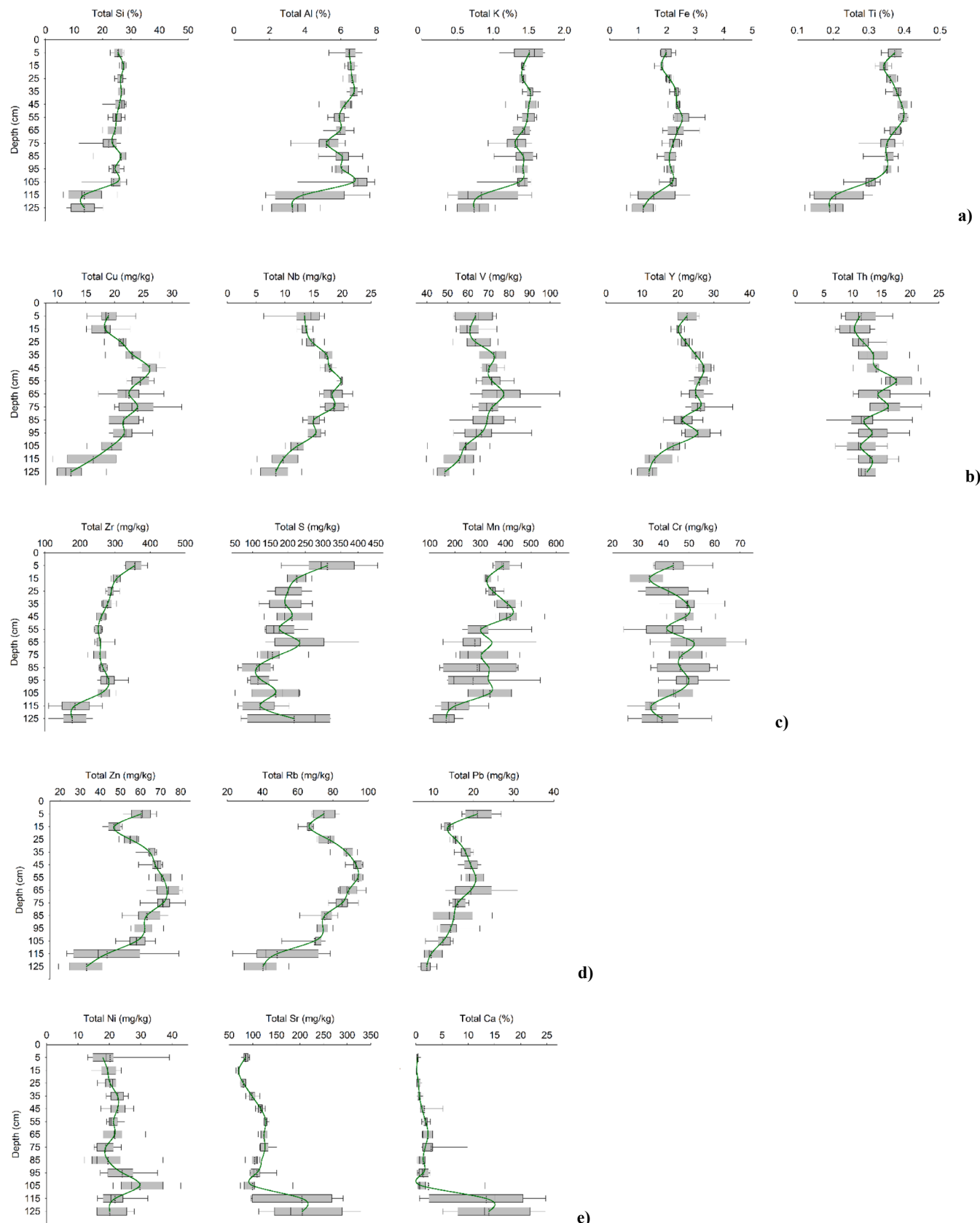


**Fig. 4.** Box-plot depth function of soil elemental content sampled at 10 cm increments for soil profile 1 in Lubbock, TX, USA. Similar distributions are given as: a) Si, Al, K, Fe, Ti; b) Cu, Nb, V, Y, Th; c) Zr, S, Mn, Cr; d) Zn, Rb, Pb; e) Ni, Sr, Ca.

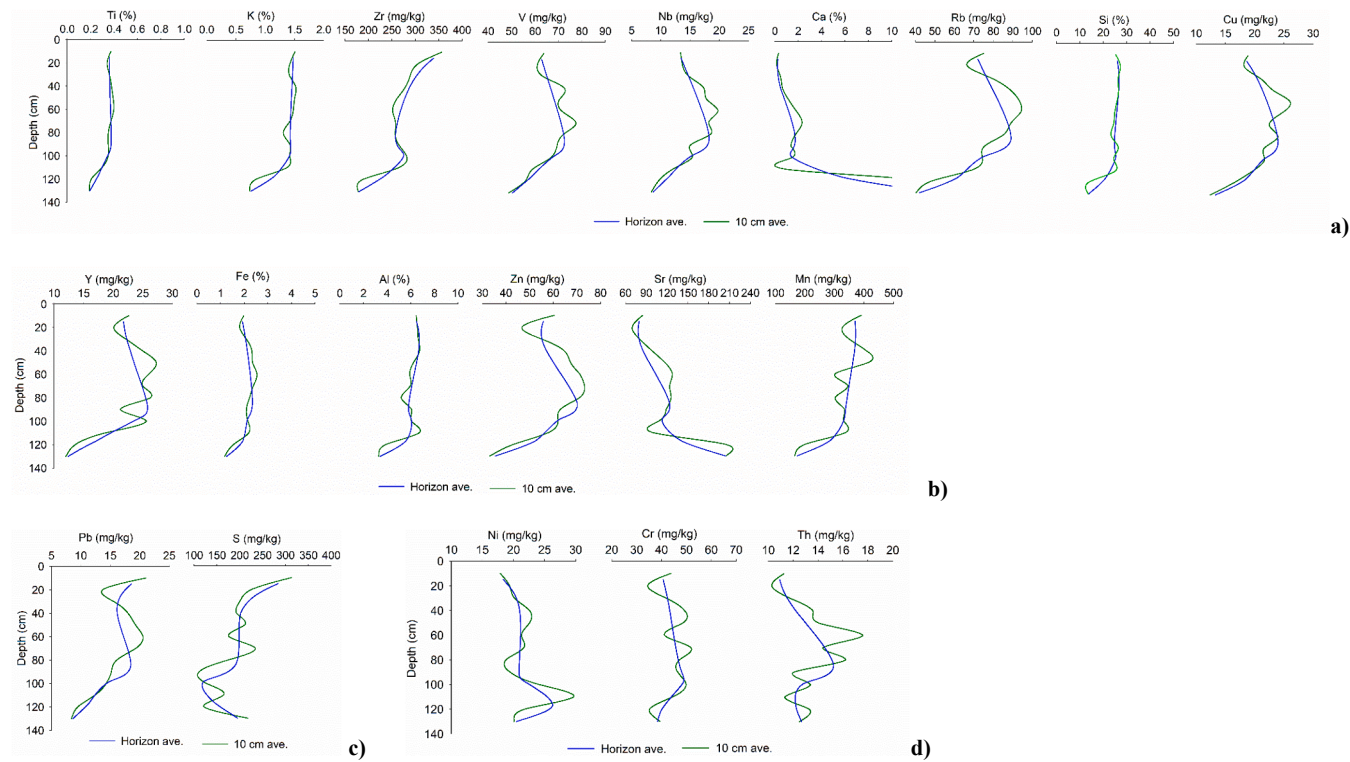


**Fig. 5.** Goodness-of-fit between elemental content of 10 cm depth layers versus six morphologically established soil horizons; soil profile 1 is in Lubbock, TX, USA. Correlations are given as follows: a)  $R^2 > 0.8$ : Ti, K, Zr, V, Nb, Ca, Rb, Si, Cu; b)  $R^2$  of 0.7 to 0.8 include Y, Fe, Al, Zn, Sr, Mn; c)  $R^2$  of 0.6 and 0.7 include Pb, S; d)  $R^2 < 0.6$  include Ni, Cr, Th.

content in the horizons of the soil, the depth function of element content provides more information by increasing the sampling density in the horizontal and vertical directions. Further, it can express the change of element content with depth, and also reflect the information such as the maximum value, minimum value, average value, and variation of element content in each layer. Also, the depth function elucidates the variability of several groups of elements differently. Note the depth function similarity among each of the following groups, yet differences between groups: 1) Si, Al, K, Fe, Ti (Fig. 4a), 2) Cu, Nb, V, Y, Th (Fig. 4b), 3) Zr, S, Mn, Cr (Fig. 4c), 4) Zn, Rb, Pb (Fig. 4d), and 5) Ni, Sr, Ca (Fig. 4e). Access to such data while describing a soil profile *in-situ* reinforces the comments of Weindorf et al. (2012) of using elemental data to augment or refine soil profile description and assessment.

### 3.3. Comparison of results by horizon and fixed depth

The aforementioned results represent the average elemental concentration values of sampling according to the six morphologically established horizons as well as the 10 cm depth-increment samples evaluation of multiple elements. To quantify the goodness-of-fit between the two curves, an R-square ( $R^2$ ) score (Nagelkerke, 1991) was calculated. The results of sampling according to morphological horizons can represent the change of an elemental content with depth. Conversely, a smaller  $R^2$  score means that the results of the two sampling methods are more inconsistent after an increase in sampling density, and the morphological sampling method from soil horizons fails to truly reflect the change of elemental content with depth.

Based upon  $R^2$  values, the elements can be divided into four groups: 1)  $R^2 > 0.8$ : Ti, K, Zr, V, Nb, Ca, Rb, Si, Cu (Fig. 5a); 2)  $R^2$  of 0.7 to 0.8 include Y, Fe, Al, Zn, Sr, Mn (Fig. 5b), (results obtained by two different sampling methods are close); 3)  $R^2$  of 0.6 and 0.7 include Pb, S (Fig. 5c); 4)  $R^2 < 0.6$  include Ni, Cr, Th (Fig. 5d). Elements in group 2 display substantive similarity between the curves, while elements in group 4 are quite different from one another. Thus for group 4

elements, the results of morphological horizon sampling do not truly reflect the change of element content with depth. In other words, not all changes in element content are consistent with changes in morphologically established soil horizons. Thus the question remains: can/should differences in elemental content be used as differentia in establishing soil profile horizons? The answer is likely rooted in the objectives of describing each individual pedon. For example, if a soil scientist is attempting to study pollutant movement into the soil with depth, establishing different horizons based upon contaminant levels may be appropriate. Yet for many standard agronomic soil profile descriptions, differentiating horizons based upon non-plant essential elements within the profile may prove time consuming and inconsequential. In some sense, perspective on this question can be traced back to the traditional adage of being a “lumper vs. splitter” (Lindbo et al., 2008). The former groups “similar features together so management implications will be similar” while the latter “create a more detailed description by recognizing subtle changes” within a soil profile.

### 3.4. Spatial distribution of elements

The depth function curve reflects the change of a certain element content with the increase of soil depth, both for evaluation by morphological soil horizons or by fixed 10 cm depths. Through *in-situ* grid testing, spatial analysis of each element was performed across the profile face using the 130 grid cells as data points. In doing so, elemental information evolves from a simple one-dimensional curve of elemental quantity with depth (Fig. 5) to a two-dimensional plane with more abundant information.

In profile 1, the spatial distribution presents four general patterns in the elemental data. First, many elements (Si, Al, K, Ti, Y, Fe, Pb, S, Zr, Mn) show low concentration at the bottom of the profile, yet are comparatively higher elsewhere (Fig. 6a). Second, some elements (Rb, Zn, V, Nb, Cu, Th) have their greatest concentration in the middle of the profile, but are lower at the bottom and top of the profile (Fig. 6b). A

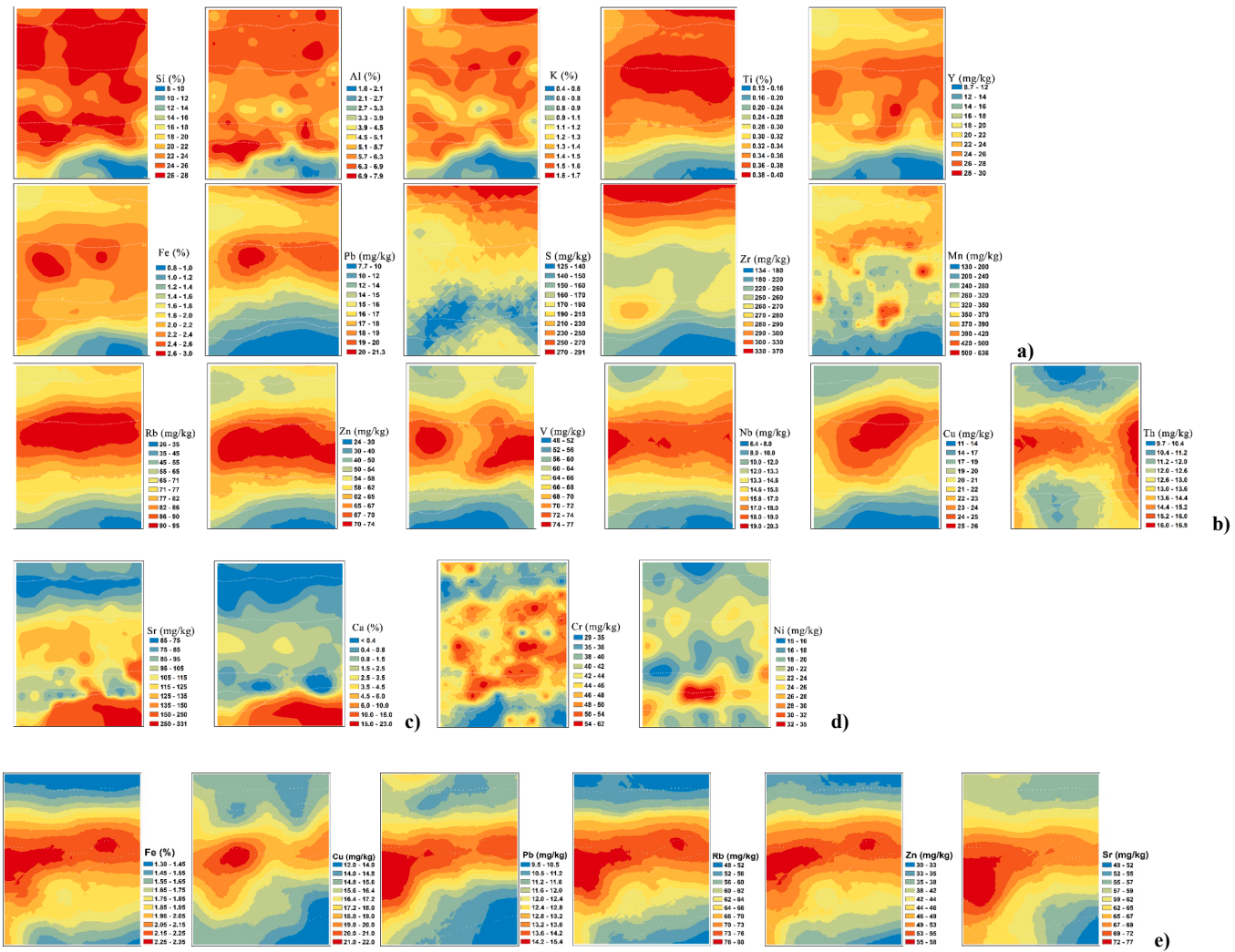


**Fig. 6.** Spatial distribution of elements across soil profiles 1 and 3 in Lubbock, TX, USA. Specifically in profile 1, a) Si, Al, K, Ti, Y, Fe, Pb, S, Zr, Mn show low concentration at the bottom of the profile, yet are comparatively higher elsewhere; b) Rb, Zn, V, Nb, Cu, Th have their greatest concentration in the middle of the profile, but are lower at the bottom and top of the profile; c) Sr and Ca are abundant deep in the profile, but comparatively low elsewhere; d) Cr and Ni showed no discernable trends with depth. By comparison in soil profile 3, e) Fe, Cu, Pb, Rb, Zn show the difference of soil horizons which are difficult to identify morphologically.

third scenario is a high concentration of certain elements (Sr, Ca) deep in the profile, but comparatively low elsewhere (Fig. 6c). Finally, a few elements (Cr, Ni) were relatively mixed throughout the profile with no discernable trends (Fig. 6d). Undoubtedly, Fig. 6b is aptly illustrating the presence of an argillic horizon within the profile while Fig. 6d is showing a calcic horizon within the profile. The presence of both of these diagnostic horizons were confirmed by field morphological description and laboratory data. Admittedly, there are significant morphological differences between horizons in profile 1. By comparison, visual morphological differences in profile 3 are not obvious; the team of soil surveyors worked for several hours before agreeing on horizonization for the profile. However, the spatial distribution of several elements obtained by PXRF proved very helpful for elucidating horizons within the profile (Fig. 6e). These findings further support the conclusions of Zhu et al. (2011) who found PXRF-determined Rb strongly associated with clay content. Given compelling evidence that PXRF can clearly aid in the identification and refinement of horizons *in-situ*, an argument can be made that field soil scientists should more strongly embrace the use of PXRF for soil pedon description. However, caution must be used when collecting PXRF data as the aperture of the instrument is only  $\sim 1.5$  cm. If the instrument is placed upon a Fe/Mn concretion,  $\text{CaCO}_3$  nodule,  $\text{CaSO}_4 \cdot 2\text{H}_2\text{O}$  crystal, etc. it could produce

inflated elemental readings relative to the overall composition of the bulk soil as a whole. To eliminate this constraint, it is advisable that the surface to be scanned is carefully examined and that multiple scans are collected from a depth of interest (or grid cell) such that the mean content of that area is considered.

### 3.5. Data visualization results

The final step of this project was the development of a data visualization tool which could overlay the PXRF elemental analysis and statistics on top of a digital photograph to ascertain to what degree elemental abundance coincides with morphological soil expression. The data visualization tool can be accessed here: <https://idatavisualizationlab.github.io/Soil/demos.html>.

The visualization tool provides several different functional areas, each of which can be manipulated to obtain different information. The user can interact with the visualization and change parameters in real time to aid in the analysis. The first component is a correlation graph to show an overview of all detected elements and their statistical relationships. A network node represents each chemical element. Links represent the relationship between nodes; the thicker the link, the stronger the correlation. Additionally, green and red links represent

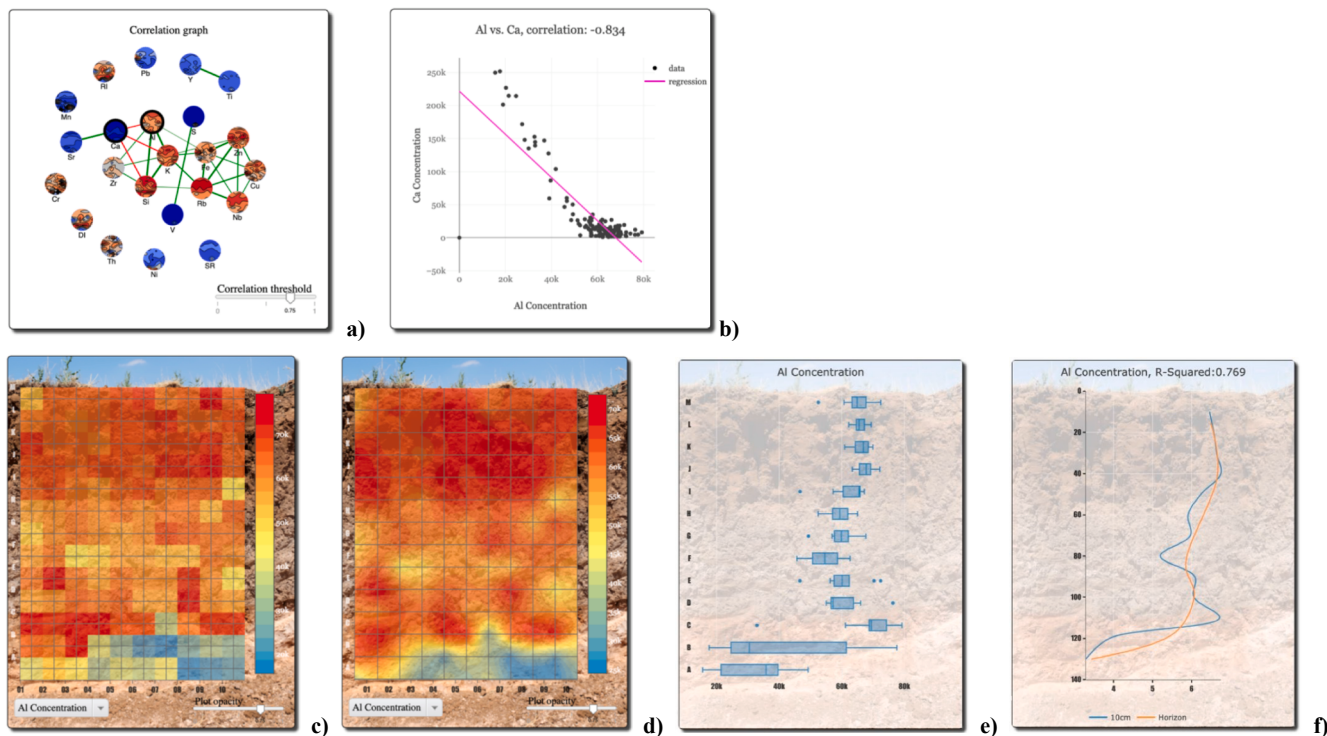


**Fig. 7.** Data visualization tool module applied to soil profile 1 in Lubbock, TX, USA. Specifically, a) green and red links represent positive and negative Pearson correlations, respectively; b) linear regression line plotted for a better understanding of the estimated correlation, with a Pearson correlation score displayed at the top of the visualization; c) rasterized contour-map of the elemental data, d) smooth contour heat map showing the distribution of the element concentration across the soil profile face. (For interpretation of the references to color in this figure legend, the reader is referred to the web version of this article.)

positive and negative Pearson correlations, respectively (Fig. 7a). The correlation threshold can be changed with a “slider” and only correlations with absolute values greater or equal to this value will be visible.

Any two of the elements can be selected to further explore their correlations. Once selected, a scatter plot is shown to display the relationship between the selected elements. Also, a linear regression line is plotted for a better understanding of the estimated correlation, with a Pearson correlation score displayed at the top of the visualization (Fig. 7b).

A rasterized contour-map (Fig. 7c) or a smooth contour heat map (Fig. 7d) can be generated based on the strings that were used to physically impose a grid across the profile, to show the distribution of the element concentration across the profile surface. Two graphs can be plotted side by side (showing different elements) for direct comparison of the chemical distributions. The smooth contour heat map can be chosen to view the discrete data measured from individual cells. Different color scales (5, 10, 20 levels) can be selected for a finer view of elemental distribution. On the right side at the bottom of the contour graphs, the plot opacity slider can be moved left and right to see the soil profile photo in the background, offering different levels of transparency for the plot data over the digital photo. On the left side at the bottom of the contour graphs, individual elements can be selected from the selection boxes and all corresponding views will be updated instantly. Grauer-Gray and Hartemink (2018) used a similar approach to evaluate three soils in Wisconsin, USA. However, their approach offered only rasterized resolution of the data, provided no instantaneous correlation between elements, and most importantly, did not offer display of the rasterized data in semi-transparency on top of a digital photograph of the profile. The approach presented herein surmounts all of those limitations, advancing the approach further.

Box-plots to show distributions of the selected elements in each 10 cm depth-increment sample of the profile are shown in Fig. 7e. Line-graphs display the goodness-of-fit between the 10 cm depth-increment samples versus the data from six morphological horizons for soil profile

assessment. To quantify this, the  $R^2$  score is also calculated and displayed at the top of the plot (Fig. 7f).

Future advancements in PXRF technology will seek to use the integrated digital camera in the aperture of the instrument to capture the soil profile photograph, divide it into a user-specified grid for scanning based on the size of the profile and resolution desired. Finally, the data visualization tool will be used to render the collected soil profile data on-site. All of this could be done using software integrated directly into the PXRF and displayed on the PXRF view screen following data acquisition. An adaptation of the approach described herein could also be applied to visualize PXRF data collected from soil cores extracted by a hydraulic probe on-site.

#### 4. Conclusions

Soil horizons are a key component of soil classification and differing from adjacent genetically related layers in physical, chemical, and biological properties or characteristics (e.g., color, structure, texture, consistency, biological organisms present, soil reaction, salinity, etc.). By visualizing the element distribution results measured by PXRF, compared with the results of traditional morphological horizonation, more abundant information can be provided. Furthermore, the spatial distribution of elements in a soil profile can be acquired quickly to obtain information that may remain visually elusive. A large amount of data can be acquired quickly and on-site, which allows for elemental data visualization in near real time.

By establishing the visualization of data correlation, element content and spatial distribution of elements in a profile, it is possible to fully understand the spatial (horizontal and vertical) distribution of soil properties. This will help to better study the distribution and migration of various elements in the soil, pedogenic development of diagnostic horizons (e.g., argillic, calcic), and/or monitor the movement of certain chemicals based upon their fundamental chemistry.

Compared with traditional soil morphological description, the

visualization of PXRF data greatly enriches the expression of elemental data in the soil profile. The creation of this soil profile data visualization tool based on PXRF data can aid in discerning the scientific implications of soil properties via rapid, *in-situ* testing. Specifically, the PXRF data visualization tool provides valuable insight into soil properties, particularly the ability to identify visually imperceptible features within soil profiles.

## Declaration of Competing Interest

The authors declare that they have no known competing financial interests or personal relationships that could have appeared to influence the work reported in this paper.

## Acknowledgements

The authors gratefully acknowledge assistance from the USDA Soil Survey Staff, namely Todd Carr, Craig Byrd, and Alain Basurco, in conducting this research. The authors gratefully acknowledge the B.L. Allen Endowment in Pedology at Texas Tech University in conducting this research. Also thanks to the National Natural Science Foundation of China (No. 41201208). The first author was supported by a scholarship under State Scholarship Fund (File No. 201708210393), China Scholarship Council.

## References

- Bakr, N., El-Ashry, S.M., 2018. Organic matter determination in arid region soils: loss-on-ignition versus wet oxidation. *Commun. Soil Sci. Plant Anal.* 49, 2587–2601.
- Bostock, M., Ogievetsky, V., Heer, J., 2011. D<sup>3</sup> data-driven documents. *IEEE Trans. Visual Comput. Graphics* 12, 2301–2309.
- Bishop, T.F.A., McBratney, A.B., Laslett, G.M., 1999. Modelling soil attribute depth functions with equal-area quadratic smoothing splines. *Geoderma* 91, 27–45.
- Cameron, A.C., Windmeijer, F.A., 1997. An R-squared measure of goodness of fit for some common nonlinear regression models. *J. Econom.* 77 (2), 329–342.
- Ceneda, D., Gschwandtner, T., May, T., Miksch, S., Schulz, H.J., Streit, M., Tominski, C., 2017. Characterizing guidance in visual analytics. *IEEE Trans. Visual Comput. Graphics* 23 (1), 111–120.
- Chakraborty, S., Weindorf, D.C., Weindorf, C.A., Das, B.S., Li, B., Duda, B., Pennington, S., Ortiz, R., 2017. Semi-quantitative evaluation of secondary carbonates via portable X-ray fluorescence spectrometry. *Soil Sci. Soc. Am. J.* 81, 844–852.
- Fu, W., Zhao, K., Zhang, C., Wu, J., Tunney, H., 2016. Outlier identification of soil phosphorus and its implication for spatial structure modeling. *Precis. Agric.* 17 (2), 121–135.
- Grauer-Gray, J., Hartemink, A.E., 2018. Raster sampling of soil profiles. *Geoderma* 318, 99–108.
- Gee, G.W., Bauder, J.W., 1986. Particle-size analysis. In: Klute, A. (Ed.), *Methods of Soil Analysis. Part 1 — Physical and Mineralogical Methods*, second ed. SSSA, Madison, WI, pp. 383–411.
- Hartemink, A.E., Minasny, B., 2014. Towards digital soil morphometrics. *Geoderma* 230–231, 305–317.
- Hu, B., Chen, S., Hu, J., Xia, F., Xu, J., Li, Y., Shi, Z., 2017. Application of portable XRF and VNIR sensors for rapid assessment of soil heavy metal pollution. *PLoS ONE*. <https://doi.org/10.1371/journal.pone.0172438>.
- Jang, M., 2010. Application of portable X-ray fluorescence (pXRF) for heavy metal analysis of soils in crop fields near abandoned mine sites. *Environ. Geochem. Health* 32 (3), 207–216.
- Kiš, I.M., 2016. Comparison of ordinary and universal kriging interpolation techniques on a depth variable (a case of linear spatial trend), case study of the Šandrovac Field. *Min.-Geol.-Pet. Eng.* 41–58. <https://doi.org/10.17794/rgn.2016.2.4>.
- Koch, J., Chakraborty, S., Li, B., Moore-Kucera, J., van Deventer, P., Daniell, A., Paul, C., Man, T., Pearson, D., Duda, B., Weindorf, C.A., Weindorf, D.C., 2017. Proximal sensor analysis of mine tailings in South Africa: an exploratory study. *J. Geochem. Explor.* 181, 45–57.
- Lemière, B., 2018. A review of pXRF (field portable X-ray fluorescence) applications for applied geochemistry. *J. Geochem. Explor.* 188, 350–363.
- Lindbo, D., Miles, R., Presley, D., Ransom, N.E., 2008. Soil profile descriptions. In: Logsdon, S., Clay, D., Moore, D., Tsegaye, T. (Eds.), *Soil Science: Step-by-Step Field Analysis*. Soil Science Society of America, Madison, WI, pp. 11–34.
- Malone, B.P., McBratney, A.B., Minasny, B., Laslett, G.M., 2009. Mapping continuous depth functions of soil carbon storage and available water capacity. *Geoderma* 154, 138–152.
- McGrath, D., Zhang, C.S., 2003. Spatial distribution of soil organic carbon concentrations in grassland of Ireland. *Appl. Geochim.* 18, 1629–1639.
- Minasny, B., Stockmann, U., Hartemink, A.E., McBratney, A.B., 2016. Measuring and modelling soil depth functions. In: Hartemink, A.E., Minasny, B. (Eds.), *Digital Soil Morphometrics*. Springer International Publishing, Cham, pp. 225–240.
- Nagelkerke, N.J., 1991. A note on a general definition of the coefficient of determination. *Biometrika* 78 (3), 691–692.
- Nelson, D.W., Sommers, L.E., 1996. Total carbon, organic carbon and organic matter. In: Sparks, D.L. (Ed.), *Methods of Soil Analysis: Chemical Methods, Part 3*. Soil Science Society of America, Madison, pp. 961–1010.
- Core Team, R., 2018. R: A Language and Environment for Statistical Computing. R Foundation for Statistical Computing, Vienna, Austria.
- Rawal, A., Chakraborty, S., Li, B., Lewis, K., Godoy, M., Paulette, L., Weindorf, D.C., 2019. Determination of base saturation percentage in agricultural soils via portable X-ray fluorescence spectrometer. *Geoderma* 338, 375–382.
- Roberts, J.C., 2007. State of the art: Coordinated & multiple views in exploratory visualization. Fifth International Conference on Coordinated and Multiple Views in Exploratory Visualization. Available online at: <https://ieeexplore.ieee.org/document/4269947> (verified 12 Apr. 2019).
- Schoeneberger, P.J., Wysocki, D.A., Benham, E.C., and Soil Survey Staff, 2012. Field book for describing and sampling soils, Version 3.0. Natl. Soil Surv. Ctr., Lincoln, NE.
- Sharma, A., Weindorf, D.C., Wang, D.D., Chakraborty, S., 2015. Characterizing soils via portable x-ray fluorescence spectrometer: 4. Cation exchange capacity (CEC). *Geoderma* 239–240, 130–134.
- Sievart, C., Parmer, C., Hocking, T., Chamberlain, S., Ram, K., Corvellec, M., Despouy, P., 2016. plotly: Create Interactive Web Graphics via 'plotly.js'. R package version, 3(0).
- Silva, S.H.G., Hartemink, A.E., Teixeira, A.F.S., Inda, A.V., Guilherme, L.R.G., Curi, N., 2018. Soil weathering analysis using portable X-ray fluorescence (PXRF) spectrometer in an Inceptisol from the Brazilian Cerrado. *Appl. Clay Sci.* 162, 27–37.
- Snedecor, G.W., Cochran, W.G., 1980. "The Sample Correlation Coefficient r" and "Properties of r." §10.1–10.2 in *Statistical Methods*, 7th ed. Iowa State Press, Ames, IA, pp. 175–178.
- Soil Survey Staff, 2006. Land resource regions and major land resource areas of the United States, Caribbean, and the Pacific Basin. USDA-NRCS. Available online at: [https://www.nrcs.usda.gov/wps/portal/nrcs/detail/soils/home/?cid=nrcs142p2\\_053624](https://www.nrcs.usda.gov/wps/portal/nrcs/detail/soils/home/?cid=nrcs142p2_053624) (verified 19 Nov. 2018).
- Soil Survey Staff, 2014a. Keys to Soil Taxonomy. USDA-NRCS. Available online at: [https://www.nrcs.usda.gov/wps/portal/nrcs/detail/soils/survey/class/?cid=nrcs142p2\\_053580](https://www.nrcs.usda.gov/wps/portal/nrcs/detail/soils/survey/class/?cid=nrcs142p2_053580) (verified 19 Nov. 2018).
- Soil Survey Staff, 2014b. Soil Survey Field and Laboratory Methods Manual. Soil Survey Investigations Report No. 51. Version 2.0. USDA-NRCS. Available at: [https://www.nrcs.usda.gov/wps/PA\\_NRCSConsumption/download?cid=stelprdb1244466&ext=pdf](https://www.nrcs.usda.gov/wps/PA_NRCSConsumption/download?cid=stelprdb1244466&ext=pdf) (verified 14 Apr. 2019).
- Stockmann, U., Cattle, S.R., Minasny, B., McBratney, A.B., 2016. Utilizing portable X-ray fluorescence spectrometry for in-field investigation of pedogenesis. *Catena* 139, 220–231.
- Thomas, G.W., 1996. Soil pH and soil acidity. In: Sparks, D.L. (Ed.), *Methods of soil analysis. Part 3. Chemical methods*. SSSA Book Ser. 5. SSSA, Madison, WI, pp. 475–490.
- US EPA, 2007. Method 6200: Field portable X-ray fluorescence spectrometry for the determination of elemental concentrations in soil and sediment. Available online at: <https://www.epa.gov/sites/production/files/2015-12/documents/6200.pdf> (verified 14 Apr. 2019).
- Weindorf, D.C., Zhu, Y., Haggard, B., Lofton, J., Chakraborty, S., Bakr, N., Zhang, W., Weindorf, W.C., Legoria, M., 2012. Enhanced pedon horizonation using portable x-ray fluorescence spectroscopy. *Soil Sci. Soc. Am. J.* 76 (2), 522–531.
- Weindorf, D.C., Bakr, N., Zhu, Y., 2014. Advances in portable X-ray fluorescence (PXRF) for environmental, pedological, and agronomic applications. *Adv. Agron.* 128, 1–45.
- Weindorf, D.C., Chakraborty, S., Aldabaa, A., Paulette, L., Corti, G., Cocco, S., Micheli, E., Wang, D., Li, B., Man, T., Sharma, A., Person, T., 2015. Lithologic discontinuity identification via proximal sensors. *Soil Sci. Soc. Am. J.* 79 (6), 1704–1716.
- Zhang, C.S., Tang, Y., Luo, L., Xu, W.L., 2009. Outlier identification and visualization for Pb concentrations in urban soils and its implications for identification of potential contaminated land. *Environ. Pollut.* 157, 3083–3090.
- Zhu, Y., Weindorf, D.C., Zhang, W., 2011. Characterizing soils using a portable x-ray fluorescence spectrometer: 1. Soil texture. *Geoderma* 167–168, 167–177.